Electronic structure and chemical boning in nonstoichiometric molecules: $Al_3X_2^-$ (X=C,Si,Ge). A photoelectron spectroscopy and *ab initio* study

Xi Li and Lai-Sheng Wang[a)]
Department of Physics, Washington State University, Richland, Washington 99352, W. R. Wiley Environmental Molecular Sciences Laboratory, Pacific Northwest National Laboratory, MS K8-88, Richland, Washington 99352

Nathan A. Cannon and Alexander I. Boldyrev[b)]
Department of Chemistry and Biochemistry, Utah State University, Logan, Utah 84322-0300

(Received 8 October 2001; accepted 31 October 2001)

The electronic and molecular structure of a series of nonstoichiometric pentaatomic species, $Al_3X_2^-$ (X=C,Si,Ge) and their corresponding neutrals, have been studied by photoelectron spectroscopy and *ab initio* calculations. Well-resolved photodetachment transitions were observed for all three species and were compared with the calculations. $Al_3C_2^-$ was found to have a $C_{2v}(^1A_1)$ global minimum with an Al^- ion coordinated to the CC triple bond in a quasi-linear AlCCAl molecule. $Al_3Si_2^-$ and $Al_3Ge_2^-$ were found to be different from the isoelectronic $Al_3C_2^-$ anion. They each have an almost planar trapezium global minimum structure with several low-lying isomers. The quasi-planarity of $Al_3Si_2^-$ and $Al_3Ge_2^-$ was understood by comparison with the previously known $SiAl_4^-$ planar molecule. © *2002 American Institute of Physics.* [DOI: 10.1063/1.1429652]

I. INTRODUCTION

Atoms in nonstoichiometric species usually are not surrounded by eight valence electrons as required by the octet rule and therefore their structures cannot be rationalized based on conventional valence theories such as the valence-shell electron-pair repulsion (VSEPR) model.[1–3] New valence models are needed in order to characterize and predict the structure of nonstoichiometric molecules. Carbon-aluminum mixed clusters have been shown to demonstrate a variety of interesting nonstoichiometric species.[4–9] Among such structures we can cite the recent discovery of tetracoordinate planar carbon in CAl_4^-,[5] CAl_5, and CAl_5^-,[6] as well as π-coordination of Al in AlC_2 and AlC_2^-.[7,8] Understanding small Al–C clusters may not only reveal novel chemical structures and bonding, but may also provide insight into bulk carbide materials. We have recently found that the Al_2C_2 neutral molecule has a quasilinear (acetylenic) structure while the $Al_2C_2^-$ anion possesses both the acetylenic and a planar-bridged structure, which are nearly degenerate.[9]

The C_2^{2-} unit is a key building block of a large number of binary and ternary metal carbides,[10,11] in particular, in carbides of electropositive elements (alkali, alkali earth, and rare earth). Yet, even though aluminum is a rather electropositive element, we are not aware of any stable solid form of aluminum carbide in the bulk with a C_2^{2-} unit. Instead bulk aluminum carbide has a stoichiometry of Al_4C_3, which reacts with water to produce methane.[10,11] Thus bulk aluminum carbide contains discrete carbon atoms, which can be viewed as C^{4-}, rather than C_2^{2-}. An interesting question is: Can a metastable bulk aluminum carbide be synthesized with C_2^{2-} as building blocks? To answer this question one need to study large clusters containing Al_xC_2 ($x>2$) and see how additional Al would interact with the CC triple bond in AlCCAl. We expect that the C–C bond will be systematically weakened with increasing Al content in Al_xC_2 and will eventually break to form what can be considered as two C^{4-} units.

The laser vaporization cluster source is a versatile experimental technique that can produce nonstoichiometric species consisting of almost any elements. Combining a laser vaporization source and negative ion photoelectron spectroscopy (PES), we have investigated a number of nonstoichiometric species. The negative ion technique offers convenient size selectivity and PES is quite suitable to provide electronic and vibrational information about the neutral species. We have found that combining PES and *ab initio* calculations is a particularly powerful approach to investigate the structure and bonding of nonstoichiometric species. In the present work we report a combined PES and *ab initio* study of $Al_3C_2^-$ and Al_3C_2 in order to understand how the extra aluminum atom may affect the CC bonding in the acetylenic Al_2C_2. We also investigated the heavier congeners, $Al_3Si_2^-$, Al_3Si_2, $Al_3Ge_2^-$, and Al_3Ge_2 and compared them with $Al_3C_2^-$ and Al_3C_2.

II. EXPERIMENT

The experiment was performed with a magnetic-bottle time-of-flight PES apparatus equipped with a laser vaporization cluster source. Details of the experimental method have been described previously.[12–15] Briefly, the $Al_3X_2^-$ (X=C,Si,Ge) anions were produced by laser vaporization of

a)Electronic mail: ls.wang@pnl.gov
b)Electronic mail: boldyrev@cc.usu.edu

the appropriate aluminum mixed targets (with graphite, Si, and Ge powders, respectively) using a pure helium carrier gas. Clusters formed from the laser vaporization source were entrained in the He carrier gas and underwent a supersonic expansion. The anion species in the beam were extracted perpendicularly into a time-of-flight mass spectrometer. Various mixed clusters composed of $Al_xX_y^-$ (X=C,Si,Ge) were formed from the source. The $Al_3X_2^-$ anions were selected in each case and decelerated before photodetachment by a laser beam. Our mass resolution ($M/\Delta M \sim 400$) was sufficient to resolve single mass differences in the cluster size range of interest. For $Al_3C_2^-$ and $Al_3Ge_2^-$, we could cleanly mass-select the desired anions for the PES experiments. However, because of the natural isotopes of Si (92.23% ^{28}Si, 4.67% ^{29}Si, 3.10% ^{30}Si) and the close mass separation between Si and Al (100% ^{27}Al), the $Al_3Si_2^-$ ion beam would always contain a small percentage of Al_4Si^- ($Al_4\,^{29}Si^-$), which we have previously investigated.[16] Thus the PES spectra of $Al_3Si_2^-$ would always contain a small contribution from that of Al_4Si^-, as shown below. For the current PES experiment, two photon energies from a Nd:YAG laser (355 and 266 nm) were used for photodetachment. The energy scales were calibrated with the known spectra of Cu^- and the electron kinetic-energy resolution of the apparatus was better than 30 meV for 1 eV electrons.

III. COMPUTATIONAL METHODS

We initially optimized the geometries and calculated frequencies of $Al_3C_2^-$, Al_3C_2, $Al_3Si_2^-$, Al_3Si_2, $Al_3Ge_2^-$, and Al_3Ge_2 employing analytical gradients with polarized split-valence basis sets (6-311+G*)[17–19] using the hybrid method, which includes a mixture of Hartree–Fock exchange with density functional exchange-correlation (B3LYP).[20–22] The geometries and frequencies were refined using the second-order Møller–Plesset perturbation theory (MP2)[23] using the same basis sets. Then, geometries of the lowest energy structures for $Al_3C_2^-$ and Al_3C_2 were refined further, using the CCSD(T)[24–26] level of theory and 6-311+G* basis sets. Finally, the energies of the lowest-energy structures were refined using the CCSD(T) level of theory and the more extended 6-311+G($2df$) basis sets. All core electrons were kept frozen in treating the electron correlation in the CCSD(T) calculations. Vertical electron detachment energies (VDEs) from the lowest-energy structures of $Al_3C_2^-$, $Al_3Si_2^-$, and $Al_3Ge_2^-$ were calculated using the outer valence Green function (OVGF) method,[27–31] as incorporated in GAUSSIAN 98. The 6-311+G($2df$) basis sets were used in all OVGF calculations, and all calculations were performed using the GAUSSIAN 98 program.[32] MO pictures were made using the MOLDEN3.4 program.[33]

IV. EXPERIMENTAL RESULTS

The PES spectra of $Al_3X_2^-$ (X=C,Si,Ge) are shown in Fig. 1 at two photon energies. The 355 nm spectrum of $Al_3C_2^-$ displayed two major detachment bands, a strong threshold band (*X*) at 2.26 eV with partially resolved vibrational features and a weaker band (*A*) at 3.23 eV binding energy. At 266 nm, the *A*-band was significantly enhanced and became the dominant feature. In addition, three more weak features (b',B,C) were observed between 3.6 and 4.4 eV.

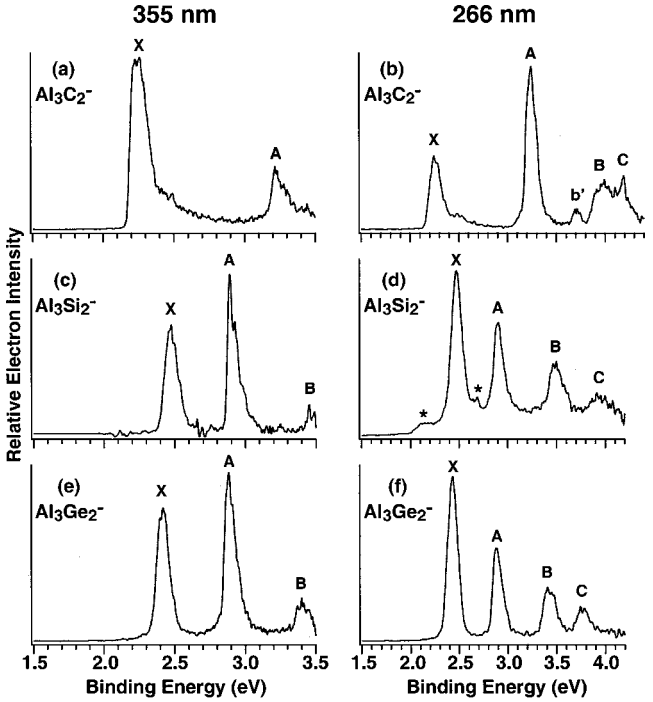

FIG. 1. Photoelectron spectra of (a) $Al_3C_2^-$ at 355 nm (3.496 eV), (b) $Al_3C_2^-$ at 266 nm (4.661 eV), (c) $Al_3Si_2^-$ at 355 nm, (d) $Al_3Si_2^-$ at 266 nm, (e) $Al_3Ge_2^-$ at 355 nm, and (f) $Al_3Ge_2^-$ at 266 nm.

The 355 nm spectrum of $Al_3Si_2^-$ [Fig. 1(c)] showed two intense bands (*X* and *A*) and a weak band (*B*), which was cut off at this photon energy. The *A*-band exhibited a partially resolved vibrational progression with a spacing of 290 (40) cm^{-1}. At 266 nm, the *B*-band was fully revealed and an additional band (*C*) was also observed. The features labeled with "*" were due to contributions from Al_4Si^- mentioned in the experimental section. In the 355 nm spectrum [Fig. 1(c)], the contributions from Al_4Si^- were cleanly subtracted, because the PES features were much better resolved at this photon energy. Although the spectra of $Al_3Si_2^-$ and $Al_3C_2^-$ are quite different, the spectra of $Al_3Ge_2^-$ [Figs. 1(e) and 1(f)] are nearly identical with those of $Al_3Si_2^-$. In addition, the $Al_3Ge_2^-$ ions could be cleanly selected, yielding PES spectra free of any contamination. The VDEs of all the observed features are given in Table I, as well as the electron affinities of the neutral species, i.e., the adiabatic detachment energies (ADEs) of the ground-state transitions.

V. THEORETICAL RESULTS

A. $Al_3C_2^-$ and Al_3C_2

We initially performed an exhaustive search for the global minimum of $Al_3C_2^-$ at the B3LYP/6-311+G* level of theory. Many structures were tested in the singlet and triplet states. A few lowest optimized structures are shown in Fig. 2. We found the lowest energy structure to be a singlet $C_{2v}(^1A_1)$ planar structure (I in Fig. 2 and Table II) with a configuration of $1a_1^2 1b_2^2 2a_1^2 3a_1^2 1b_1^2 2b_2^2 4a_1^2 5a_1^2 3b_2^2$. Upon

TABLE I. Observed vertical (VDE) and adiabatic (ADE) detachment energies in eV from the photoelectron spectra of $Al_3C_2^-$, $Al_3Si_2^-$, and $Al_3Ge_2^-$.

	VDE	ADE
	$Al_3C_2^-$	
X	2.26 (0.03)	2.19 (0.03)
A	3.23 (0.03)	
b′	3.71 (0.03)	
B	3.96 (0.06)	
C	4.19 (0.05)	
	$Al_3Si_2^-$	
X	2.47 (0.03)	2.43 (0.03)
A	2.89 (0.03)	
B	3.50 (0.05)	
C	3.95 (0.06)	
	$Al_3Ge_2^-$	
X	2.42 (0.03)	2.36 (0.03)
A	2.88 (0.03)	
B	3.46 (0.04)	
C	3.81 (0.05)	

TABLE II. Calculated molecular properties of $Al_3C_2^-$.

$Al_3C_2^-$, C_{2v}, $^1A_1$	B3LYP/6-311+G*	MP2/6-311+G*	CCSD(T)/6-311+G*[a]
$R(C_1-C_2)$, Å	1.285	1.314	1.305
$R(C_1-Al_3)$, Å	2.175	2.142	2.162
$R(C_1-Al_4)$, Å	1.963	1.961	1.965
$R(Al_3-Al_4)$, Å	2.940	2.881	2.894
$<C_1C_2Al_5^\circ$	163.2	161.2	161.4
$<C_1Al_3C_2Al_5^\circ$	0.0	0.0	0.0
$-E_{tot}$, au	803.567 16	801.903 47	801.959 33
$\omega_1(a_1)$, cm^{-1}	1731	1661	
$\omega_2(a_1)$, cm^{-1}	438	493	
$\omega_3(a_1)$, cm^{-1}	332	344	
$\omega_4(a_1)$, cm^{-1}	129	148	
$\omega_5(a_2)$, cm^{-1}	230	170	
$\omega_6(b_1)$, cm^{-1}	82	71	
$\omega_7(b_2)$, cm^{-1}	639	657	
$\omega_8(b_2)$, cm^{-1}	478	483	
$\omega_9(b_2)$, cm^{-1}	206	231	

[a]Frequencies were not calculated at this level of theory.

further refinement at the MP2/6-311+G* level of theory, the C_{2v} ($^1A_1$) structure was found to be a minimum again (Table II). We, therefore, concluded that the single C_{2v} planar structure is the global minimum. Further examination of this structure at the CCSD(T)/6-311+G* level of theory revealed the same geometric parameters as at the B3LYP/6-311+G* and MP2/6-311+G* levels of theory. Therefore, we used the B3LYP/6-311+G* and MP2/6-311+G* levels of theory for geometry optimization and frequency calculations for the heavier $Al_3Si_2^-$, Al_3Si_2, $Al_3Ge_2^-$, and Al_3Ge_2 species.

Upon electron detachment from the highest occupied molecular orbital (HOMO) ($3b_2$, Fig. 3) of $Al_3C_2^-$, the corresponding neutral C_{2v} Al_3C_2 ($^2B_2$) was found to be a minimum at the B3LYP/6-311+G* level of theory with the $1a_1^2 1b_2^2 2a_1^2 3a_1^2 1b_1^2 2b_2^2 4a_1^2 5a_1^2 3b_2^1$ electronic configuration (Table III). However, upon further refinement at the MP2/6-311+G* level of theory, the C_{2v} ($^2B_2$) structure was found to be a saddle point (Table III). Geometry optimization

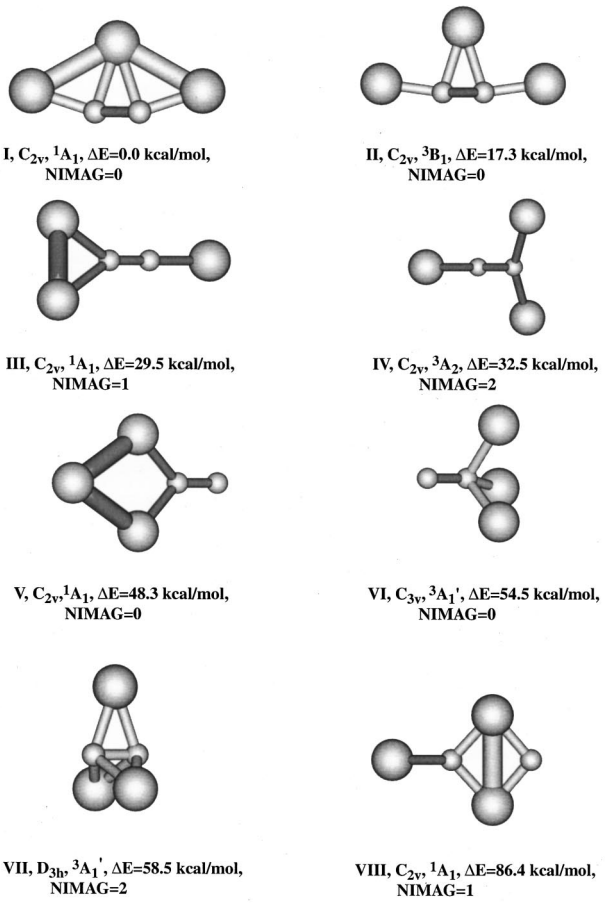

FIG. 2. Selected structures of $Al_3C_2^-$ optimized at the B3LYP/6-311+G* level of theory.

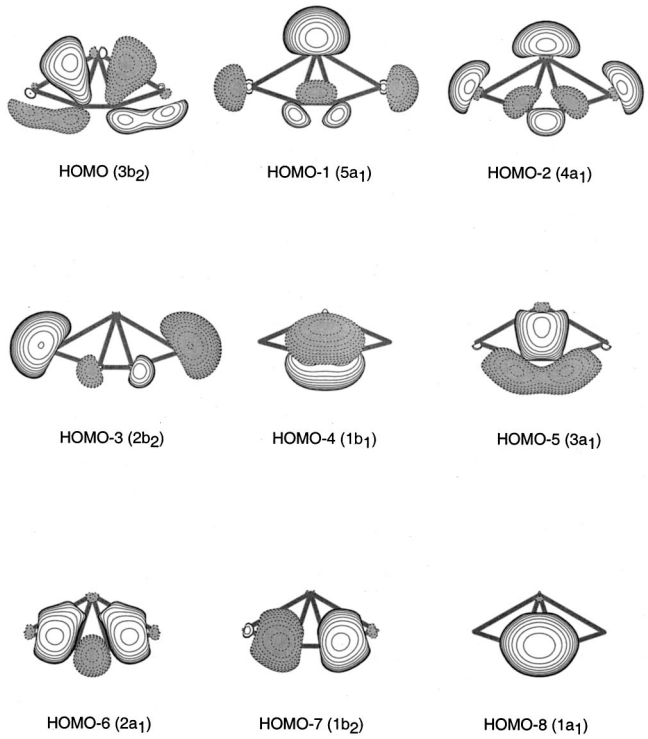

FIG. 3. Valence molecular orbital pictures (Ref. 33) of $Al_3C_2^-$.

TABLE III. Calculated molecular properties of Al_3C_2.

Al_3C_2, C_{2v}, $^2B_2$	B3LYP/ 6-311+G*	MP2/[a] 6-311+G*	Al_3C_2, C_2, ^2B	MP2/ 6-311+G*	CCSD(T)/ 6-311+G* [a]
$R(C_1-C_2)$, Å	1.262	1.287	$R(C_1-C_2)$, Å	1.287	1.281
$R(C_1-Al_3)$, Å	2.261	2.201	$R(C_1-Al_3)$, Å	2.201	2.230
$R(C_1-Al_4)$, Å	2.023	2.012	$R(C_1-Al_4)$, Å	2.012	2.020
$R(Al_3-Al_4)$, Å	3.162	3.318	$R(Al_3-Al_4)$, Å	3.317	3.145
$<C_1C_2Al_5^c$	168.7	176.8	$<C_1C_2Al_5^c$	175.1	168.1
$<C_1Al_3C_2Al_5^c$	0.0	0.0	$<C_1Al_3C_2Al_5^c$	176.2	176.2
$-E_{tot}$, au	803.490 79	801.826 94	$-E_{tot}$, au	801.826 95	801.889 56
$\omega_1(a_1)$, cm^{-1}	1870	1808	$\omega_1(a)$, cm^{-1}	1808	
$\omega_2(a_1)$, cm^{-1}	375	419	$\omega_2(a)$, cm^{-1}	420	
$\omega_3(a_1)$, cm^{-1}	267	329	$\omega_3(a)$, cm^{-1}	333	
$\omega_4(a_1)$, cm^{-1}	51	92	$\omega_4(a)$, cm^{-1}	173	
$\omega_5(a_2)$, cm^{-1}	170	124 i	$\omega_5(a)$, cm^{-1}	92	
$\omega_6(b_1)$, cm^{-1}	65	76	$\omega_6(b)$, cm^{-1}	615	
$\omega_7(b_2)$, cm^{-1}	539	613	$\omega_7(b)$, cm^{-1}	370	
$\omega_8(b_2)$, cm^{-1}	220	341	$\omega_8(b)$, cm^{-1}	78	
$\omega_9(b_2)$, cm^{-1}	40	62	$\omega_9(b)$, cm^{-1}	77	

[a]Frequencies were not calculated at this level of theory.

following the normal mode of the imaginary frequency resulted in a C_2 (^2B) global minimum structure. The Al–C–C–Al fragment of the C_2 Al_3C_2 molecule is slightly zigzag (out of plane), distorted similarly to what we previously found for Al_2C_2 (C_{2h}).[9] However, the distortion from planarity was found to be very small and the vibrationally averaged structure is actually planar. Further examination of this structure at the CCSD(T)/6-311+G* level of theory gave similar results as at the MP2/6-311+G* level.

The $Al_3C_2^-$ anion was found to be very stable relative to fragmentation. We calculated that $D_e=74.1$ kcal/mol for $Al_3C_2^-$ (C_{2v}, $^1A_1$) $\rightarrow Al_2C_2$ (C_{2h}, ^1A_g) + Al^- (^3P). The substantial stability of the anion is due to the bonding between the CC unit and the Al ligands as well as the bonding interactions among the ligand Al atoms. Upon electron detachment from the HOMO, primarily of Al–Al and C–Al bonding characters (Fig. 3), the stability of the Al_3C_2 neutral molecule dropped substantially: $D_e=39.0$ kcal/mol for Al_3C_2 (C_{2v}, $^2B_2$) $\rightarrow Al_2C_2$(C_{2h}, ^1A_g) + Al(^2P) (all at the CCSD(T)/6-311+G(2*df*)//CCSD(T)/6-311+G* levels of theory).

For $Al_3C_2^-$ (C_{2v}, $^1A_1$) we tested our OVGF results using three basis sets, 6-311+G*, 6-311+G(2*d*), and 6-311+(2*df*), as well as geometries optimized at the B3LYP/6-311+G*, MP2/6-311+G*, and CCSD(T)/6-311+G* levels of theory. As shown in Table IV, using the geometry at the B3LYP/6-311+G* level does not affect the calculated photoelectron spectra by more than 0.05 eV, and all the calculated VDEs agree with the experimental results within 0.2 eV. We believe that a similar agreement with experiment can be expected for the heavier systems currently under consideration. At our highest level of theory, the calculated vertical and adiabatic electron detachment energies for the $Al_3C_2^-$ (C_{2v}, $^1A_1$) ground state were: VDE =2.25 eV [OVGF/6-311+G(2*df*)] and ADE=2.15 eV [CCSD(T)/6-311+G(2*df*)], which agree excellently with the experimental data: VDE=2.26 (0.03) eV and ADE=2.19 (0.03) eV (Table I).

B. $Al_3Si_2^-$, Al_3Si_2, $Al_3Ge_2^-$, and Al_3Ge_2

We first performed an exhaustive search for the global minimum of $Al_3Si_2^-$ at the B3LYP/6-311+G* level of theory. Many structures were tested in the singlet and triplet states and a few low-energy structures are shown in Fig. 4. The lowest energy structure was found to be a singlet C_s ($^1A'$) trapezium-planar structure (Fig. 4 and Table V). Upon further refinement at the MP2/6-311+G* level of theory, the C_s ($^1A'$) structure was found to be a first-order saddle point (Table V) and the global minimum structure was

TABLE IV. Comparison of the calculated and experimental electron detachment processes of $Al_3C_2^-$.

	Experiment VDE (eV)	$Al_3C_2^-$ Electron detachment from MO	Theory[a] VDE (eV) OVGF/ 6-311+G*// B3LYP/ 6-311+G*	Theory[a] VDE (eV) OVGF/ 6-311+G(2*d*)// B3LYP/ 6-311+G*	Theory[a] VDE (eV) OVGF/ 6-311+G(2*df*)// B3LYP/ 6-311+G*	Theory[a] VDE (eV) OVGF/ 6-311+G(2*df*)// MP2/ 6-311+G*	Theory[a] VDE (eV) OVGF/ 6-311+G(2*df*)// CCSD(T)/ 6-311+G*
X	2.26 (0.03)	$3b_2$	2.00 (0.88)	2.12 (0.87)	2.19 (0.87)	2.29 (0.87)	2.25 (0.87)
A	3.23 (0.03)	$5a_1$	3.24 (0.86)	3.33 (0.86)	3.36 (0.86)	3.27 (0.86)	3.30 (0.86)
B	3.96 (0.06)	$4a_1$	3.92 (0.85)	4.01 (0.85)	4.04 (0.85)	4.04 (0.85)	4.06 (0.85)
C	4.19 (0.05)	$2b_2$	4.22 (0.83)	4.31 (0.83)	4.34 (0.83)	4.40 (0.84)	4.39 (0.84)

[a]Pole strength is given in parentheses.

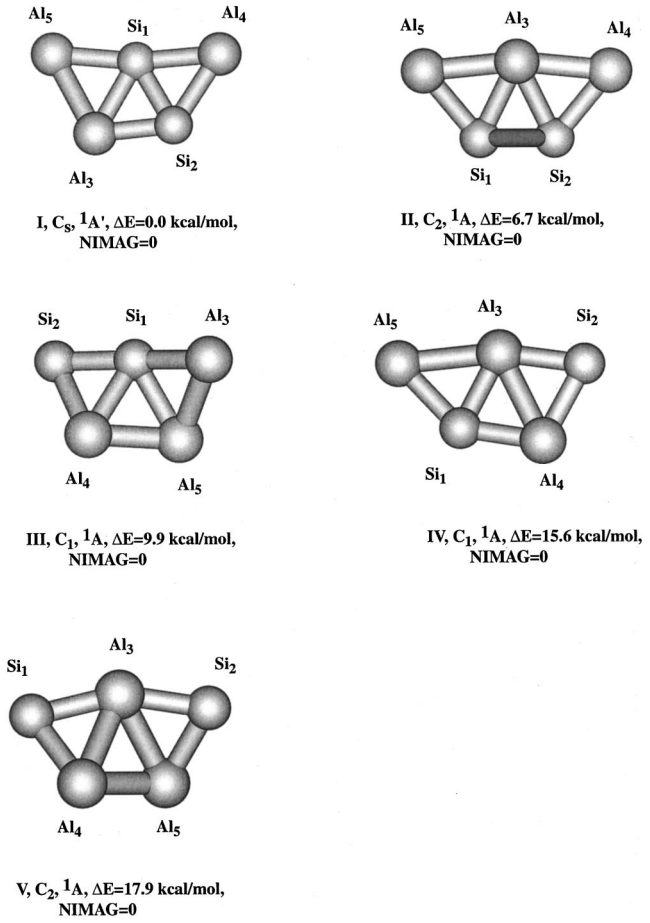

FIG. 4. Selected structures of $Al_3Si_2^-$ optimized at the B3LYP/6-311+G* level of theory.

found to be slightly nonplanar (C_1). However, the planarization barrier is comparable with the difference in zero-point energy (ZPE) corrections between the planar and nonplanar structures. Therefore, the vibrationally averaged structure of $Al_3Si_2^-$ should be planar. For $Al_3Ge_2^-$, the planar C_s ($^1A'$) structure was found to be the global minimum at both the B3LYP/6-311+G* and MP2/6-311+G* levels of theory (Table VI). The analog of the global minimum of the C_{2v} $Al_3C_2^-$ structure was found to be the lowest-lying isomer for both the $Al_3Si_2^-$ and $Al_3Ge_2^-$ anions.

Neutral structures for Al_3Si_2 and Al_3Ge_2 derived from the most stable structures of their anions by detaching an electron from their HOMO have also been optimized at B3LYP/6-311+G* and were found to be minima (Tables V and VI). However, at the MP2 and CCSD(T) levels of theory their wave functions were found to be heavily spin-contaminated and therefore ADEs were not calculated for the $Al_3Si_2^-$ and $Al_3Ge_2^-$ anions. At our highest level of theory, the calculated VDEs are: 2.48 eV for $Al_3Si_2^-$ (C_1, ^1A) and 2.44 eV for $Al_3Ge_2^-$ (C_1, ^1A), both at OVGF/6-311+G($2df$). These theoretical values are again in excellent agreement with the experimental data: VDE=2.47±0.03 eV for $Si_2Al_3^-$ and 2.42±0.03 eV for $Al_3Ge_2^-$ (Table I).

VI. INTERPRETATION OF THE PHOTOELECTRON SPECTRA

A. $Al_3C_2^-$

In Table IV we present the results of our calculations of the four major low lying vertical one-electron detachment processes from the C_{2v} ($^1A_1$) global minimum structure of $Al_3C_2^-$. The experimental VDEs are also listed in Table IV for comparison.

1. Band X

The VDE of band *X* (Fig. 1) at 2.26 eV agrees well with the calculated VDE of 2.25 eV [OVGF/6-311+G($2df$)/CCSD(T)/6-311+G*] by removing an electron from the $3b_2$-HOMO of the global minimum $Al_3C_2^-$ structure. Our calculated ADE of 2.15 eV [CCSD(T)/6-311+G($2df$)] is also in excellent agreement with the experi-

TABLE V. Calculated molecular properties of $Al_3Si_2^-$ and Al_3Si_2.

$Al_3Si_2^-$ C_s, $^1A'$	B3LYP/ 6-311+G*	MP2/ 6-311+G*	$Al_3Si_2^-$ C_1, ^1A	MP2/ 6-311+G*	Al_3Si_2 C_s, $^2A'$	B3LYP/ 6-311+G*
R(Si_1-Si_2), Å	2.302	2.299	R(Si_1-Si_2), Å	2.301	R(Si_1-Si_2), Å	2.376
R(Si_1-Al_3), Å	2.567	2.525	R(Si_1-Al_3), Å	2.529	R(Si_1-Al_3), Å	2.416
R(Si_1-Al_4), Å	2.577	2.554	R(Si_1-Al_4), Å	2.552	R(Si_1-Al_4), Å	2.469
R(Si_1-Al_5), Å	2.587	2.558	R(Si_1-Al_5), Å	2.546	R(Si_1-Al_5), Å	2.599
$<Si_2Si_1Al_3^\circ$	59.6	60.1	$<Si_2Si_1Al_3^\circ$	60.1	$<Si_2Si_1Al_3^\circ$	58.9
$<Al_4Si_1Si_2^\circ$	64.5	64.0	$<Al_4Si_1Si_2^\circ$	64.0	$<Al_4Si_1Si_2^\circ$	61.8
$<Al_5Si_1Al_3^\circ$	65.8	65.7	$<Al_5Si_1Al_3^\circ$	65.6	$<Al_5Si_1Al_3^\circ$	70.6
$<Si_1Al_4Si_2Al_3^\circ$	0.0	0.0	$<Si_1Al_4Si_2Al_3^\circ$	−8.0	$<Si_1Al_4Si_2Al_3^\circ$	0.0
$<Si_1Al_5Al_3Si_2^\circ$	0.0	0.0	$<Si_1Al_5Al_3Si_2^\circ$	14.6	$<Si_1Al_5Al_3Si_2^\circ$	0.0
$-E_{tot}$, au	1306.410 88	1303.969 08	$-E_{tot}$, au	1303.969 57	$-E_{tot}$, au	1306.326 89
ω_1(a′), cm^{-1}	463	478	ω_1(a), cm^{-1}	477	ω_1(a′), cm^{-1}	442
ω_2(a′), cm^{-1}	397	418	ω_2(a), cm^{-1}	417	ω_2(a′), cm^{-1}	376
ω_3(a′), cm^{-1}	342	372	ω_3(a), cm^{-1}	370	ω_3(a′), cm^{-1}	356
ω_4(a′), cm^{-1}	265	281	ω_4(a), cm^{-1}	283	ω_4(a′), cm^{-1}	284
ω_5(a′), cm^{-1}	248	266	ω_5(a), cm^{-1}	267	ω_5(a′), cm^{-1}	208
ω_6(a′), cm^{-1}	172	210	ω_6(a), cm^{-1}	211	ω_6(a′), cm^{-1}	199
ω_7(a′), cm^{-1}	110	126	ω_7(a), cm^{-1}	136	ω_7(a′), cm^{-1}	92
ω_8(a″), cm^{-1}	70	64	ω_8(a), cm^{-1}	74	ω_8(a″), cm^{-1}	97
ω_9(a″), cm^{-1}	42	85 i	ω_9(a), cm^{-1}	56	ω_9(a″), cm^{-1}	27

TABLE VI. Calculated molecular properties of $Al_3Ge_2^-$ and Al_3Ge_2.

$Al_3Ge_2^-$ C_5, $^1A'$	B3LYP/ 6-311+G*	MP2/ 6-311+G*	Al_3Ge_2 C_5, $^2A'$	B3LYP/ 6-311+G*
$R(Ge_1-Ge_2)$, Å	2.476	2.491	$R(Ge_1-Ge_2)$, Å	2.553
$R(Ge_1-Al_3)$, Å	2.638	2.631	$R(Ge_1-Al_3)$, Å	2.583
$R(Ge_1-Al_4)$, Å	2.627	2.639	$R(Ge_1-Al_4)$, Å	2.528
$R(Ge_1-Al_5)$, Å	2.671	2.657	$R(Ge_1-Al_5)$, Å	2.667
$<Ge_2Ge_1Al_3^\circ$	57.8	58.3	$<Ge_2Ge_1Al_3^\circ$	57.4
$<Al_4Ge_1Ge_2^\circ$	63.2	62.9	$<Al_4Ge_1Ge_2^\circ$	60.7
$<Al_5Ge_1Al_3^\circ$	62.5	62.5	$<Al_5Ge_1Al_3^\circ$	68.2
$<Ge_1Al_4Ge_2Al_3^\circ$	0.0	0.0	$<Ge_1Al_4Ge_2Al_3^\circ$	0.0
$<Ge_1Al_5Al_3Ge_2^\circ$	0.0	0.0	$<Ge_1Al_5Al_3Ge_2^\circ$	0.0
$-E_{tot}$, au	4881.460 60	4876.806 02	$-E_{tot}$, au	4881.379 28
$\omega_1(a')$, cm^{-1}	334	337	$\omega_1(a')$, cm^{-1}	318
$\omega_2(a')$, cm^{-1}	286	300	$\omega_2(a')$, cm^{-1}	277
$\omega_3(a')$, cm^{-1}	266	279	$\omega_3(a')$, cm^{-1}	261
$\omega_4(a')$, cm^{-1}	226	234	$\omega_4(a')$, cm^{-1}	231
$\omega_5(a')$, cm^{-1}	200	210	$\omega_5(a')$, cm^{-1}	183
$\omega_6(a')$, cm^{-1}	131	156	$\omega_6(a')$, cm^{-1}	154
$\omega_7(a')$, cm^{-1}	95	106	$\omega_7(a')$, cm^{-1}	83
$\omega_8(a'')$, cm^{-1}	52	51	$\omega_8(a'')$, cm^{-1}	79
$\omega_9(a'')$, cm^{-1}	25	17	$\omega_9(a'')$, cm^{-1}	17

mental ADE of 2.19 eV. The $3b_2$-HOMO (Fig. 3) of $Al_3C_2^-$ is of C–C antibonding character with bonding C–Al and Al–Al interactions. Table III shows that the C–C bond length is slightly shortened in the Al_3C_2 neutral, whereas the C–Al and Al–Al bond lengths are increased. These geometry changes between the ground states of the anion and the neutral are consistent with the nature of the HOMO. Table III also shows that under C_2 symmetry there are five totally symmetric modes (a), which could be active during photodetachment. These modes range in frequencies from as low as 92 cm^{-1} to 1808 cm^{-1} for the C–C stretching at MP2/6-311+G*. Fine features in the 355 nm spectrum were discernible, as shown in Fig. 1(a). However, the fact that so many modes could be active prevented us from resolving a simple vibrational progression. The feature around 2.5 eV, which was recognizable in both the 355 and 266 nm spectra was consistent with the frequency of the C–C stretching mode, which was expected to be active.

2. Band A

The second vertical electron detachment takes place from the $5a_1$ orbital (HOMO-1, Fig. 3) with a theoretical VDE of 3.30 eV [OVGF/6-311+G(2*df*)/CCSD(T)/6-311+G*] (Table IV). This theoretical VDE agrees well with the second detachment feature (*A*), which was observed with a VDE of 3.23 eV (Fig. 1). The $5a_1$ orbital is primarily a combination of Al lone pairs with a weak C–C bonding interaction (Fig. 3). Electron detachment from this MO should not lead to a large geometry change, consistent with the relatively narrow PES band observed experimentally.

3. Bands b′, B, and C

The third and fourth detachment channels occur from removing electrons from the $4a_1$ (HOMO-2) and $2b_2$ (HOMO-3), respectively, as shown in Fig. 3. The calculated VDEs for these two channels at OVGF/6-311+G(2*df*)/CCSD(T)/6-311+G* level of theory are 4.06 and 4.39 eV, respectively. However, the observed PES spectrum [Fig. 1(b)] in this energy range was surprisingly complicated with three resolved features, the weak band *b′* at a VDE of 3.71 eV, a broad band *B* at a VDE of 3.96 eV, and an apparently sharp band *C* at a VDE of 4.19 eV. The *B* and *C* bands overlapped and were not well resolved. The theoretical VDEs for the third and fourth detachment channels are in very good agreement with the *B* and *C* bands, respectively. In particular, the $2b_2$ orbital is almost a pure Al lone pair orbitals with a very slight C–C antibonding character and should correspond to the sharp *C* band. This leaves the weak *b′* band unaccounted for. Impurities could be ruled out because the mass spectrum was clean and the resolution was sufficient to distinguish any impurity contributions. Anion isomers could also be ruled out since there was no low-lying isomers identified from our extensive theoretical search. The lowest isomer was still 17.3 kcal/mol higher (Fig. 2). There are two possible interpretations for the weak feature *b′*. First, it could be due to a shake-up process, i.e., a two-electron transition. Alternatively, it could be due to the 0–0 transition for the *B* band. The latter interpretation would indicate that the *B* band has a vibrational progression in the C–C stretching mode with the $\nu=1$ level at around 3.96 eV. The difference between this VDE and the 3.71 eV VDE of the *b′* band yields a vibrational spacing of about 2000 cm^{-1}. Although the $4a_1$ orbital is mainly a combination of Al lone pairs, it has a reasonable C–C bonding character (Fig. 3). Thus, activities in this mode upon photodetachment would not be too surprising. However, at the current level of theory we could not definitively assign the weak *b′* feature.

B. $Al_3Si_2^-$ and $Al_3Ge_2^-$

We consider the assignments of the PES features for $Al_3Si_2^-$ and $Al_3Ge_2^-$ together because their spectra were nearly identical (Fig. 1), indicating the two anions should

TABLE VII. Comparison of calculated and experimental electron detachment processes of $Al_3Si_2^-$ and $Al_3Ge_2^-$.

Feature	Experiment VDE (eV)	Electron detachment from MO	Theory[a] VDE (eV) C_1, ^1A
		$Al_3Si_2^-$	
X	2.47	9a	2.48 (0.87)
A	2.89	8a	2.96 (0.87)
B	3.50	7a	3.64 (0.86)
C	3.95	6a	3.88 (0.86)
		$Al_3Ge_2^-$	
X	2.42	9a	2.44 (0.87)
A	2.88	8a	2.93 (0.87)
B	3.46	7a	3.45 (0.86)
C	3.81	6a	3.68 (0.87)

[a]At the OVGF/6-311+G(2*df*)//MP2/6-311+G* level of theory. Pole strength is given in parentheses.

have similar structures and bonding, which were born out from our theoretical calculations (Tables V and VI). In Table VII we present the results of our calculations of the four major low-lying vertical one-electron detachment processes from the C_I ($^1A'$) structures of $Al_3Si_2^-$ and $Al_3Ge_2^-$ together with the experimental data for comparison.

The assignments and interpretation of the PES spectra for $Al_3Si_2^-$ and $Al_3Ge_2^-$ are straightforward according to the calculations. Four well-resolved detachment bands were observed for each system and they correspond to removing an electron from the top four MOs from the global minimum structure of the anion. The valence MOs for $Al_3Si_2^-$ are shown in Fig. 5 and they exhibit more complicated shapes and patterns due to the lower symmetry of the anion. The valence MOs for $Al_3Ge_2^-$ are similar and are not shown. The calculated VDEs for the top four detachment channels are given in Table VII for $Al_3Si_2^-$ and $Al_3Ge_2^-$. The pole strengths in all the calculated detachment channels, given in parentheses, are larger than 0.8, indicating that the OVGF method is valid and all the electron detachments can be considered as primarily one-electron processes. In each case, the theoretical results are in almost perfect agreement with the experimental data. The VDEs from the lowest-lying isomer, which is analogous to the global minimum of $Al_3C_2^-$, do not agree with the experimental data, suggesting that indeed the structure of $Al_3Si_2^-$ and $Al_3Ge_2^-$ is different from their lighter congener.

The overall agreement between the experimental PES spectra and the theoretical calculations for all three species is quite satisfying, confirming the structures of these species predicted computationally.

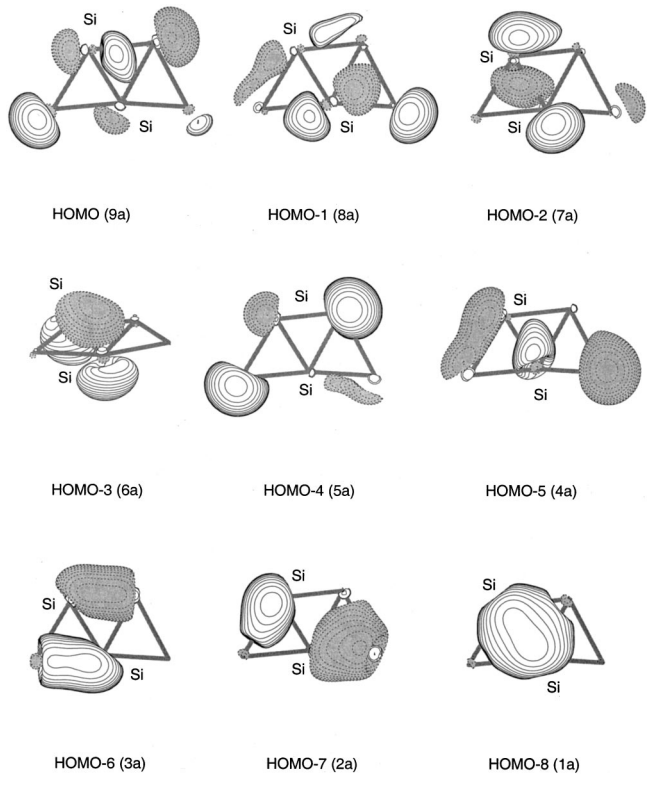

FIG. 5. Valence molecular orbital pictures (Ref. 33) of $Al_3Si_2^-$.

VII. CHEMICAL BONDING IN $Al_3C_2^-$ AND Al_3C_2

In our previous study on Al_2C_2, we found that the planar-bridged structure (D_{2d}) is a third order saddle point, the nonplanar bridged-structure (C_{2v}) is a second order saddle point, and the vinylidene-like structure ($Al_2C{=}C$) is a first order saddle point.[9] Only the quasi-linear acetylenic structure (AlC≡CAl) is a minimum. The deviation from a perfect linear structure of the acetylenic Al_2C_2 was attributed to a second order effect due to mixing with low-lying excited states. The extra electron in the acetylenic $Al_2C_2^-$ anion resulted in a degenerate electronic state ($^2\Pi_g$) under the $D_{\infty h}$ symmetry. The anion was also found slightly nonlinear. However, we stress that vibrationally averaged structures are essentially linear for both the anion and neutral species. The $Al_2C_2^-$ anion also has a planar-bridged D_{2h} isomer, which was found to be 7.2 kcal/mol higher in energy at our highest level of theory [CCSD(T)/6-311+G(2*df*)] and was observed experimentally, even though the neutral D_{2h} Al_2C_2 is a third-order saddle point.

The canonical order of the occupied valence MOs in the 14-valence electron quasilinear Al_2C_2 (C_{2h},^1A_g) is $1a_g^2 1b_u^2 2a_g^2 1a_u^2 2b_u^2 3b_u^2 3a_g^2 1b_g^0$. The canonical order of the occupied valence MOs in the planar-bridged (D_{2h},^1A_g) structure is $1a_g^2 1b_{1u}^2 1b_{2u}^2 2a_g^2 1b_{3u}^2 3a_g^2 2b_{1u}^2 1b_{3g}^0$.

Occupation of the lowest unoccupied molecular orbital (LUMO) ($1b_g$) of Al_2C_2 in the quasilinear anion should lead to a shortening of the Al–C bond and an elongation of the C–C bond in $Al_2C_2^-$, because of the antibonding C–C π-character and the bonding C–Al π-character of the $1b_g$ MO. Occupation of the LUMO ($1b_{3g}$) in the planar-bridged isomer should lead to similar structural effects in the anion, because it also has an antibonding C–C π-character and a bonding C–Al π-character. Indeed we found such structural changes in the optimized structures between the anion and the neutral molecule. Based on this MO analysis one would expect that the structures of Al_3C_2 and $Al_3C_2^-$ would be a combination of the linear and rhombus structures. That is indeed what we found from our extensive geometrical search. The additional Al atom is attached to the C–C bond

in the quasi-linear Al_2C_2, resulting in additional Al–Al and Al–C bonding interactions.

The overall bonding in Al_3C_2 and $Al_3C_2^-$ can be interpreted rather easily based on the MO picture shown in Fig. 3. The $1a_1$ MO (HOMO-8) is a C–C σ-bond. The $1b_2$ (HOMO-7) and $2a_1$ (HOMO-6) orbitals represent linear combinations of two C–Al σ-bonds. The $3a_1$ MO (HOMO-5) is originated from the in-plane C–C π-bond and represents a σ-bonding interaction between the bridging Al and C_2. This bonding interaction weakens the C–C bond, leading to the lengthened C–C bond in $Al_3C_2^-$ compared to the C–C bond in the quasi-linear $C–Al_t$ and Al_2C_2. The $1b_1$ MO (HOMO-4) is the out-of-plane C–C π-bond. The $2b_2$ (HOMO-3), $4a_1$ (HOMO-2), and $5a_1$ (HOMO-1) orbitals are primarily linear combinations of the Al $3s$ lone pairs. The $3b_2$ HOMO mainly represents the $C–Al_t$ and $Al_t–Al_b$ bonding interactions between the terminal and bridging Al with a slight C–C anti-bonding character. When one electron is detached from the HOMO, the $Al_t–Al_b$ bonding is weakened substantially (stability towards dissociation dropped by 35 kcal/mol) and the Al–Al bond length is increased substantially (by 0.36 Å, see Table II). Thus, the C–C bond in $Al_3C_2^-$ can be viewed as a double bond, compared to the acetylenic triple bond in Al_2C_2. Therefore, the weakening of the C–C bond with the additional Al is vividly revealed. It is expected that further addition of Al in the $Al_xC_2^-$ cluster series will eventually lead to the break of the C–C bond and formation of separated C^{4-} unit, characteristic of bulk aluminum carbide.

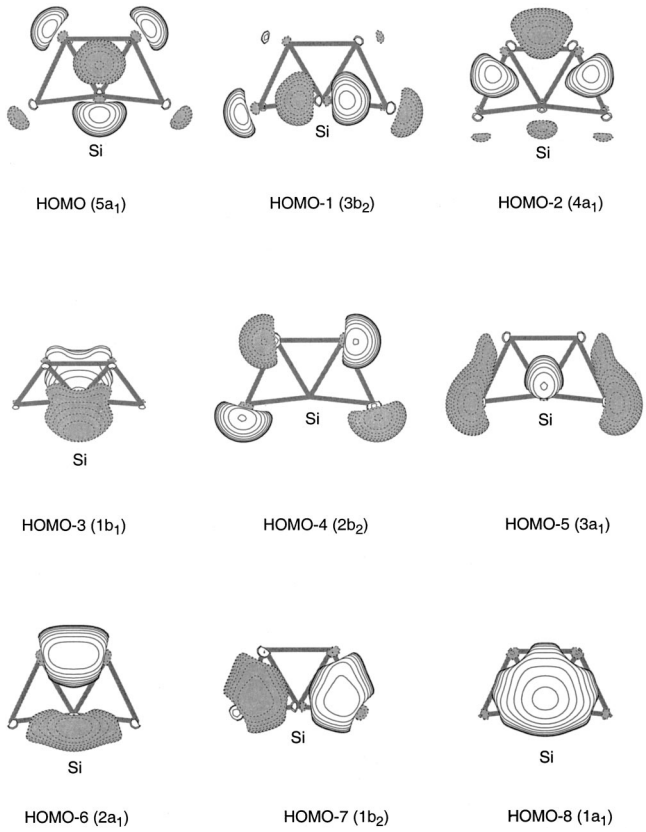

FIG. 6. Valence molecular orbital pictures (Ref. 33) of $SiAl_4^-$.

VIII. CHEMICAL BONDING IN $Al_3Si_3^-$, Al_3Si_2, $Al_3Ge_2^-$, AND Al_3Ge_2

The molecular orbitals of $Al_3Si_2^-$, Al_3Si_2, $Al_3Ge_2^-$, and Al_3Ge_2 cannot be easily interpreted due to their low symmetry and mixing of bonding and lone-pair orbitals, as shown in Fig. 5 for $Al_3Si_2^-$. However, the Al_3Si_2 and Al_3Ge_2 neutral species are valent isoelectronic with the $SiAl_4^-$ and $GeAl_4^-$ anions that we studied previously.[16] Both $SiAl_4^-$ and $GeAl_4^-$ were shown to have a trapezoidal structure, which was confirmed by comparison of theoretical VDEs with the experimental PES data. The trapezoidal structure for $SiAl_4^-$ and $GeAl_4^-$ was understood and rationalized by comparing with the first pentaatomic tetracoordinate molecule, CAl_4^-.[5]

The structure and MOs of $SiAl_4^-$ are presented in Fig. 6. We can see immediately that the geometries of Al_3Si_2 and Al_3Ge_2 are very similar to the trapezoidal $SiAl_4^-$ if we substitute an Al^- by Si or Ge. Therefore, we can use the MOs shown in Fig. 6 for the more symmetric $SiAl_4^-$ to interpret and understand the structures of Al_3Si_2 and Al_3Ge_2. The presence of the three-center peripheral Al–Al bond in $SiAl_4^-$ and $GeAl_4^-$ was shown previously to be critical for the planarity of these species,[16] as well as the planarity of the pentaatomic tetracoordinate planar carbon molecules.[5,34,35] While it is hard to exactly identify that kind of multicenter peripheral bond in Al_3Si_2 and Al_3Ge_2 due to the mixing of the MOs, we can assume, based on the isoelectronic nature between Al_3Si_2 and $SiAl_4^-$, that the resulting effects from orbital interactions would be similar in Al_3Si_2 as in $SiAl_4^-$. Hence a planar structure found for Al_3Si_2 and Al_3Ge_2 is understandable. When an extra electron is added to form the $Al_3Si_2^-$ and $Al_3Ge_2^-$ anions, the anion structures are not expected to be very different from the neutral species and that is indeed what we found in our calculations.

IX. CONCLUSIONS

We report a combined experimental and theoretical investigation of the structures and bonding in a series of nonstoichiometric molecules, $Al_3C_2^-$, $Al_3Si_2^-$, $Al_3Ge_2^-$ and their corresponding neutral species. Photoelectron spectra of the anions were measured and electron detachment energies from several MOs of the anions were obtained. While all the three species are valent isoelectronic, the structure and bonding of the C-containing species were found to be very different from the Si- or Ge-containing species. The $Al_3C_2^-$ and Al_3C_2 molecules can be considered as an AlCCAl acetylenic species interacting with an additional Al through π-coordination to the CC bond. All three Al atoms can be viewed as Al^+ as a result of their donating their single p electron to the CC group, which has charges of C_2^{4-} in $C_2Al_3^-$ and C_2^{3-} in C_2Al_3. The CC bond is weakened (close to a CC double bond), due to the filling of the anti-bonding CC π-bond ($3b_2$-HOMO, Fig. 3) by the additional electron from the third Al atom. The geometric and electronic structure of Al_3Si_2 and Al_3Ge_2 species was interpreted based on the geometric and electronic structure of their isoelectronic $SiAl_4^-$ and $GeAl_4^-$ anions. Based on this analogy we concluded that peripheral bonding interactions are responsible

for the planar (or quasi-planar) trapezium structures of $Al_3Si_2^-$, Al_3Si_2, $Al_3Ge_2^-$, and Al_3Ge_2, as are the cases in $SiAl_4^-$ and $GeAl_4^-$.

ACKNOWLEDGMENTS

The theoretical work was done at Utah State University and partially supported by The Petroleum Research Fund (ACS-PRF# 35255-AC6), administered by the American Chemical Society. The experimental work done in Washington was supported by the National Science Foundation (DMR-0095828) and performed at the W. R. Wiley Environmental Molecular Sciences Laboratory, a national scientific user facility sponsored by DOE's Office of Biological and Environmental Research and located at Pacific Northwest National Laboratory, which is operated for DOE by Battelle under Contract DE-AC06-76RLO 1830.

[1] C. M. Day, Jr. and J. Selbin, *Theoretical Inorganic Chemistry*, 2nd ed. (Reinhold, New York, 1969).
[2] R. J. Gillespie, *Molecular Geometry* (Van Nostrand-Reinhold, London, 1972).
[3] D. L. Kepert, *Inorganic Stereochemistry, Inorganic Chemistry Concepts*, Vol. 6 (Springer, Berlin, 1982).
[4] A. I. Boldyrev, J. Simons, X. Li, W. Chen, and L. S. Wang, J. Chem. Phys. **110**, 8980 (1999).
[5] X. Li, L. S. Wang, A. I. Boldyrev, and J. Simons, J. Am. Chem. Soc. **121**, 6033 (1999).
[6] A. I. Boldyrev, J. Simons, X. Li, and L. S. Wang, J. Chem. Phys. **111**, 4993 (1999).
[7] A. I. Boldyrev, J. Simons, X. Li, W. Chen, and L. S. Wang, J. Am. Chem. Soc. **121**, 10193 (1999).
[8] L. S. Knight, Jr., S. T. Cobranchi, O. Herlong, and C. A. Arrington, J. Chem. Phys. **92**, 5856 (1990).
[9] N. A. Cannon, A. I. Boldyrev, X. Li, and L. S. Wang, J. Chem. Phys. **113**, 2671 (2000).
[10] A. F. Wells, *Structural Inorganic Chemistry*, 5th ed. (Clarendon, Oxford, 1984).
[11] F. A. Cotton and G. Wilkinson, *Advanced Inorganic Chemistry*, 5th ed. (Wiley, New York, 1988).
[12] L. S. Wang, in *Photoionization and Photodetachment*, edited by C. Y. Ng (World Scientific, Singapore, 2000), Vol. 10, Chap. 16.
[13] X. Li and L. S. Wang, J. Chem. Phys. **111**, 8389 (1999).
[14] L. S. Wang, H. S. Cheng, and J. Fan, J. Chem. Phys. **102**, 9480 (1998).
[15] L. S. Wang and H. Wu, in *Advances in Metal and Semiconductor Clusters. IV. Cluster Materials*, edited by M. A. Duncan (JAI, Greenwich, 1998), pp. 299–343.
[16] A. I. Boldyrev, X. Li, and L. S. Wang, Angew. Chem. Int. Ed. Engl. **39**, 3307 (2000).
[17] A. D. McLean and G. S. Chandler, J. Chem. Phys. **72**, 5639 (1980).
[18] T. Clark, J. Chandrasekhar, G. W. Spitznagel, and P. v. R. Schleyer, J. Comput. Chem. **4**, 294 (1983).
[19] M. J. Frisch, J. A. Pople, and J. S. Binkley, J. Chem. Phys. **80**, 3265 (1984).
[20] R. G. Parr and W. Yang, *Density-functional Theory of Atoms and Molecules* (Oxford University Press, Oxford, 1989).
[21] A. D. Becke, J. Chem. Phys. **96**, 2155 (1992).
[22] J. P. Perdew, J. A. Chevary, S. H. Vosko, K. A. Jackson, M. R. Pederson, D. J. Singh, and C. Fiolhais, Phys. Rev. B **46**, 6671 (1992).
[23] R. Krishnan, J. S. Binkley, R. Seeger, and J. A. Pople, J. Chem. Phys. **72**, 650 (1980).
[24] J. Cizek, Adv. Chem. Phys. **14**, 35 (1969).
[25] G. D. Purvis III and R. J. Bartlett, J. Chem. Phys. **76**, 1910 (1982).
[26] G. E. Scuseria, C. L. Janssen, and H. F. Schaefer III, J. Chem. Phys. **89**, 7382 (1988).
[27] L. S. Cederbaum, J. Phys. B **8**, 290 (1975).
[28] W. von Niessen, J. Shirmer, and L. S. Cederbaum, Comput. Phys. Rep. **1**, 57 (1984).
[29] V. G. Zakrzewski and J. V. Ortiz, Int. J. Quantum Chem., Quantum Chem. Symp. **28**, 23 (1994).
[30] V. G. Zakrzewski and J. V. Ortiz, Int. J. Quantum Chem. **53**, 583 (1995).
[31] J. V. Ortiz, V. G. Zakrzewski, and O. Dolgunitcheva, in *Conceptual Trends in Quantum Chemistry*, edited by E. S. Kryachko (Kluwer, Dordrecht, 1997), Vol. 3, p. 463.
[32] M. J. Frisch, G. M. Trucks, H. B. Schlegel *et al.* GAUSSIAN 98, Revision A.7, Gaussian, Inc., Pittsburgh PA, 1998.
[33] MO pictures were made using MOLDEN3.4 program. G. Schaftenaar, MOLDEN3.4, CAOS/CAMM Center, The Netherlands (1998).
[34] L. S. Wang, A. I. Boldyrev, X. Li, and J. Simons, J. Am. Chem. Soc. **122**, 7681 (2000).
[35] X. Li, H. F. Zhang, L. S. Wang, G. D. Geske, and A. I. Boldyrev, Angew. Chem. Int. Ed. Engl. **39**, 3630 (2000).